Colloid Polym Sci (2007) 285:1301–1311
DOI 10.1007/s00396-007-1708-7

ORIGINAL CONTRIBUTION

On the formation of calcium carbonate thin films under Langmuir monolayers of stearic acid

Michael Maas · Heinz Rehage · Holger Nebel · Matthias Epple

Received: 6 December 2006 / Revised: 30 May 2007 / Accepted: 31 May 2007 / Published online: 13 July 2007

Abstract In this publication, we describe the growth of thin films of calcium carbonate beneath Langmuir monolayers of stearic acid. The size and shape of the crystalline structures were systematically studied by means of different microscopic techniques including Brewster angle microscopy, atomic force microscopy and scanning electron microscopy. In a series of experiments, we explored the calcium carbonate crystallization process for different lipid monolayers and subphases. The observed phenomena support a crystallization process which is induced by a thin, film-like structure of a precursor phase. The basic processes of crystal and aggregate formation can be represented by a simple model which is based on electrostatic interactions between the surfactant film and the inorganic calcium carbonate structures.

Keywords Biomineralization · Precursor film · Calcium carbonate · Stearic acid · Brewster angle microscopy

Introduction

Biomineralization is a natural process that finally leads to the formation of complex nano-structured materials. These special structures are assembled by highly controlled growth mechanisms at the organic/inorganic interface [1–5]. Extensive research in the field of biomineralization is not only important for the comprehension of the processes in nature but could also lead to the development of advanced techniques for the architecture of new materials. A straightforward attempt which can be used to study biomineral growth is based on the application of Langmuir films. These lipid monolayers provide a simple model system for the organic/inorganic interface present in biomineralization, e.g. membranes or protein surfaces. Calcium carbonate is the most important biomineral, being present, e.g. in mollusc shells, skeletons of foraminiferes and coccolithophores or corals (see [6] for a recent review).

At the beginning of the 1990s, Heywood and Mann [7] demonstrated that the morphology of calcium carbonate ($CaCO_3$) crystals can be controlled by the choice of the surfactants (here: fatty acids) which were spread onto an aqueous $CaCO_3$-forming subphase [8, 9]. The observed phenomena were explained by the occurrence of lattice matching between the polar head groups of the surfactant and the crystal lattice of the $CaCO_3$-crystals. This kind of heterogeneous crystallization is known as epitaxy in crystallography. Besides these phenomena, crystallization is controlled by a delicate interplay between thermodynamics (lattice energy) and kinetics (nucleation and growth). Recent studies questioned the role of thermodynamically controlled nucleation process and suggested a kinetic model [10–13]. In the framework of these models, the supersaturation of ions near the interface plays an important role in understanding the nucleation process. In addition, the occurrence of epitaxy was also questioned because lattice matching does not seem to occur until the formation of the initial crystals has taken place [10]. In close analogy to homogeneous crystallization processes in the aqueous phase [14], an amorphous precursor phase at the interface was postulated [15–17]. From this precursor phase, the

M. Maas (✉) · H. Rehage
Physical Chemistry II, University of Dortmund,
44227 Dortmund, Germany
e-mail: michael.maas@uni-dortmund.de

H. Nebel · M. Epple
Institute of Inorganic Chemistry, University of Duisburg-Essen,
45117 Essen, Germany

different crystal modifications should emerge, depending on the external conditions [16, 18–24].

Different mechanisms for these processes were suggested involving self-assembly of nanoparticles (for reviews see [15, 25]) but up to this point, there is only limited experimental evidence for the existence of such an amorphous precursor phase in vitro [26, 27], although it could be prepared in large scale in vitro by crystallization from aqueous $Ca(OH)_2$ and gaseous CO_2 at low temperature [28, 29].

Many studies focused on the effects of additives (like mollusc shell matrix extracts [30–43], polyelectrolytes [29, 44–46], proteins [47, 48] or block copolymers [49]) on the crystallization of biominerals in suitable bulk crystallization experiments. In this paper, we report the formation of $CaCO_3$ crystals beneath Langmuir monolayers. First, this phenomenon was observed by measuring the spreading properties of stearic acid monolayers on a calcium hydrogencarbonate [$Ca(HCO_3)_2$] subphase. Subsequently, Brewster angle microscopy (BAM) allowed the analysis of the growth of calcium carbonate single crystals and also of the formation of cohesive thin films of calcium carbonate [50, 51]. In this approach, we take on these studies and add further insights gained by the application of the presented techniques.

We also present a simple model which can describe the basic steps of this film formation. In a series of experiments, we investigated Langmuir films of stearic acid, stearylamine, stearylalcohol, dimyristoylphosphatidylcholine (DMPC) and tricosa-10,12-diynedioic acid (TCDA). From these experiments, we could determine the influence of the polar head groups on the formation of the $CaCO_3$ films. In most cases, a calcium hydrogencarbonate solution was used as a subphase. To investigate the influence of primary particles, we also investigated subphases of aqueous dispersions of Silica Ludox© beads. In addition to optical BAM measurements, we investigated the ultra-thin films by different techniques including light microscopy, atomic force microscopy (AFM), scanning electron microscopy (SEM), and X-ray powder diffraction (XRD).

Materials and methods

Substances

All substances were purchased at analytical grade from Sigma-Aldrich and used without further purification. The sodium salt of stearylsulfate was treated with excess HCl to form the free acid. The lipids were dissolved in chloroform at concentrations of 1 mM. In a series of experiments, we investigated surface-active compounds like stearic acid, stearylalcohol, stearylamine, DMPC, TCDA and stearylsulfate. Silica Ludox™ Beads were obtained from a 2.2 g/cm^3 stock solution (10 wt%, pH=9.3, zeta potential=−38±1 mV, mean particle size=28±5 nm, 0.01 mol/l KCl).

Preparation of the $Ca(HCO_3)_2$ solutions

For the preparation of the $Ca(HCO_3)_2$ solutions, several grams of $CaCO_3$ were suspended in 0.5 l water and flushed with gaseous CO_2 for about 2 h. To remove excess $CaCO_3$, the solution was filtered. In addition, the solutions were filtered again before each application. The concentration of the $Ca(HCO_3)_2$ solutions prepared by this method was approximately 8 mM [determined by titration with ethylenediaminetetraacetic acid (EDTA)]. The pH of this solution was 7.2.

BAM experiments

For all experiments, a Langmuir–Blodgett trough (NIMA-Technology, Coventry, England, Type 601 BAM) was filled with 200 ml of water (Elsa Purelab Ultra, 18.2 MΩ). Afterwards, the organic surfactant solution was spread on the water surface. After evaporation of the solvent chloroform (about 5 min), the lipid monolayer was compressed until a solid-condensed film occurred with Π_o (surface pressure)≈25 mN m^{-1}. To generate well-defined domain structures, the solid condensed film was expanded and compressed several times. Afterwards, the 8-mM solution of $Ca(HCO_3)_2$ was induced into the subphase by means of a perfusor pump, and the excess water was simultaneously removed to obtain a constant water level. The induction speed was 25 ml h^{-1} so that a homogeneous distribution of the ions in the subphase could be reached by diffusion. This was done to ensure a controlled monitoring of the crystallization processes. Experiments at which the lipids were directly spread onto the subphase were performed as well, but there it was difficult to observe the first crystallization steps. Overall, the results of these simpler experiments were equivalent to the infusion technique. In similar experiments, 180 mg ml^{-1} Silica Ludox© (mean particle size, 28±5 nm; zeta potential, −38±1 mV) dispersion was introduced into the subphase. During all these experiments, the water surface was monitored by BAM.

Light microscopy

For investigations of light microscopy, a few drops of 4 mM $Ca(HCO_3)_2$ solution were put on a glass slide (hydrophilic) with concave cavities. Thus, a smooth water surface without a meniscus could be achieved. Afterwards, a single droplet of the lipid, dissolved in chloroform, was spread at the surface of the aqueous phase. After evaporation of the chloroform, we investigated the structures emerging on the drop surface by light microscopy with an Olympus BX50 instrument.

Atomic force microscopy

For AFM, the lipid solution was spread onto a 4-mM Ca $(HCO_3)_2$ solution. The lipid was compressed until a solid condensed film was obtained ($\Pi_o \approx 25$ mN m^{-1}). Then, using the Langmuir–Blodgett technique, a thin sheet of a graphite substrate was attached at an angle of 50° onto a dipper and dipped (dipping speed, 1 mm/min) into the solution. Afterwards, the surface was sucked clean, and the dipper was pulled out again quickly. The substrate was rinsed with water in order to remove any larger crystals and dried under argon. The samples were observed with a scanning force microscope (Nanowizard, JPK-Instruments, Berlin) in tapping mode, using a silicon cantilever tip with a bending spring constant of 29–61 N/m (manufacturer specified; Nanosensors Switzerland) oscillating close to its resonance frequency (302–382 kHz). The scan rate was 1 Hz, and the applied force was at its minimum.

Scanning electron microscopy

For scanning electron microscopy, 150 µl stearic acid (1 mM) was spread onto 400 ml of a 6-mM $Ca(HCO_3)_2$ solution in a Langmuir–Blodgett trough. The films were compressed to surface pressures of about 30 mN m^{-1}. At a specified time (see Table 2) after the surface pressure was obtained (approximately 30 min after the beginning of the experiment), the films were transferred by the same technique as described at the above paragraph. The substrates were not rinsed with water; on the contrary, it was ensured to quickly remove remaining water droplets from the surface. As substrate, a silicon wafer was applied, which was made hydrophobic. For this purpose, silicon wafers were aligned next to a drop of dimethyldichlorsilane, left in an exsiccator overnight and afterwards were washed with freshly distilled acetone. Different samples were prepared at temperatures between 5 and 40 °C. At 20 °C, additional samples were prepared at different $Ca(HCO_3)_2$ concentrations. The growth time and the pH were varied (for a summary, see Table 2). These samples were investigated by a FEI ESEM Quanta 400 scanning electron microscope which was equipped with energy-dispersive X-ray spectroscopy (EDAX EDS Genesis 4000).

X-ray powder diffractometry

The crystallized material was collected by scratching off the crystals from hydrophobized silicon wafers (obtained as described above) and then studied in transmission mode on a Kapton foil with a Siemens D5000 diffractometer using CuK_α radiation (λ=1.54 Å). Because of the small amounts of crystallized material, it was only possible to collect sufficient material from experiments carried out at room temperature. Additionally, one sample was measured with pure $CaCO_3$ powder [the same as used for the preparation of the $Ca(HCO_3)_2$ solution].

Results and discussion

In analogy to recent experiments performed by Hacke [50, 51], we investigated the crystallization of $CaCO_3$ under a monolayer of stearic acid. If stearic acid is quickly spread onto an aqueous subphase of calcium hydrogencarbonate, thin films of $CaCO_3$ emerge in direct proximity to the Langmuir film.

In the aqueous subphase, the following equilibrium reaction occurs:

$$CaCO_3(s)+H_2O(l)+CO_2(g)\,\acute{o} \leftrightarrow Ca(HCO_3)_2(aq) \qquad (1)$$

This reaction also takes place during natural mineralization processes. This simple membrane system is, therefore, well suited to model biomineralization.

In the following, only these phenomena are shown that are linked to the formation of thin films or precursor aggregates. In almost all cases, a large amount of calcite single crystals sooner or later appeared together with those structures and eventually fall to the ground of the reaction vessel. The formation of such calcite crystals is well documented in the literature [7–9, 52–54] and shall only be discussed in this paper if it contributes to the understanding of the observed processes.

X-ray powder diffractometry

Figure 1 shows a powder diffractogram obtained from a sample prepared at T=20 °C, $[Ca(HCO_3)_2]$=6 mM, t_{growth}= 1.5 h, Π_o=30 mN m^{-1}. In this paper, the two polymorphs calcite and vaterite could be identified. Compared to the sample with pure $CaCO_3$, the diffractogram exhibits a strong amorphous region. Other diffractograms of samples at 20 °C differed in the relative reflection intensities, i.e. the ratio of calcite to vaterite, but showed these two phases only. Thus, we tentatively assume that all objects found by SEM and proven by energy dispersive X-ray (EDX) to be $CaCO_3$ are either calcite, vaterite or possibly X-ray amorphous phases (like amorphous calcium carbonate; ACC) by visual comparison of the structures.

Brewster angle microscopy

The thin $CaCO_3$ film which was formed under the Langmuir monolayer of stearic acid could easily be investigated by means of BAM. For monolayers of stearylalcohol, stearylamine, DMPC, DMP and stearylsulfate at comparable

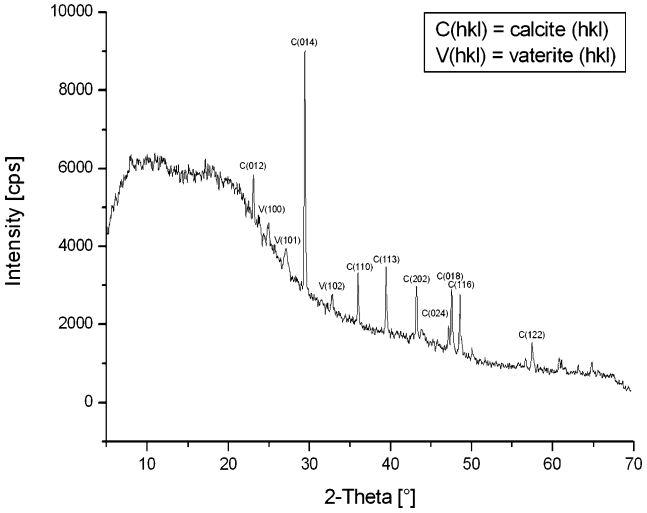

Fig. 1 X-ray powder diffractogram taken from a sample at T=20 °C, [$Ca(HCO_3)_2$]=6 mM, t_{growth}=1.5 h, Π_o=30 mN m^{-1} below a stearic acid monolayer

conditions (solid condensed films, same $Ca(HCO_3)_2$ concentration), we obtained completely different results. Typical BAM-images are shown in Figs. 2 and 3. For the latter lipids, it is evident that only isolated crystals were formed. The special crystallization processes for the formation of such crystals were already studied in detail earlier [7–9, 52–54]. The basic factors—like the kind of headgroups involved, hydrophobic chain length, surface pressure, temperature, etc.—responsible for the growth of calcite, vaterite and aragonite were shown in these studies, but a satisfactory understanding of the growth mechanisms of these crystals is still lacking.

In a series of different experiments, we could observe extensive crystal formation only under densely packed monolayers of stearic acid. We conclude that the nature of the polar surfactant head group has a strong influence on the formation of $CaCO_3$ crystals. To get more information on the crystallization mechanism, we studied the kinetics of aggregate formation below monolayers of stearic acid.

Fig. 2 Typical $CaCO_3$ aggregates formed below the stearic acid monolayer, observed by Brewster angle microscopy (BAM; Π_o= 35 mN m^{-1}, T=20 °C, [$Ca(HCO_3)_2$]=2 mM, pH=7)

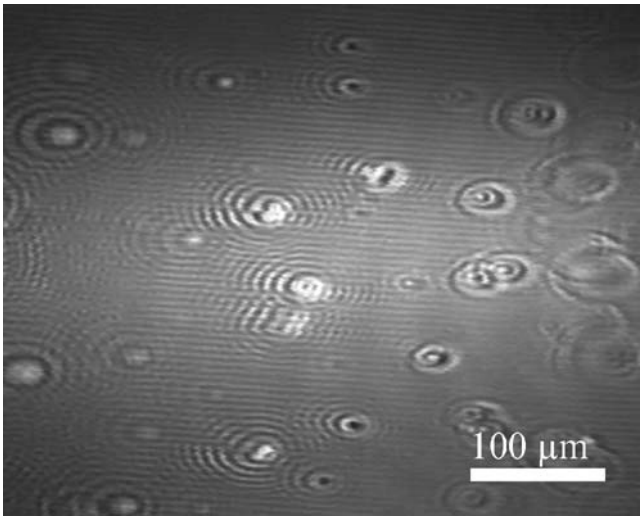

Fig. 3 Isolated $CaCO_3$ crystals formed below a stearylalcohol monolayer, observed by BAM. The crystals are so small that only scattering rings can be observed (Π_o=35 mN m^{-1}, T=20 °C, [$Ca(HCO_3)_2$]=2 mM, pH=7)

Typical results are shown in Fig. 4. In this experiment, 50 ml of an 8-mM aqueous solution of $Ca(HCO_3)_2$ was introduced into the subphase during 2 h (starting concentration, 0 mM; final concentration, 2 mM). Immediately after the beginning of the experiment, first particles with a diameter around 200 nm (the maximimum lateral resolution) formed at defects of the monolayer (Fig. 4a). These defects appeared as bright dots which were present already before the $Ca(HCO_3)_2$ solution was induced (Fig. 4a). The calcium carbonate particles appear as white dots and could only be differentiated by extensive blank tests with pure water or calcium chloride as subphase. Consecutively, these particles started to form fractal aggregates (Fig. 4b). With increasing time [accordingly increasing the $Ca(HCO)_3)_2$ concentration], the aggregates became more densely packed (Fig. 4c), until finally, a thin closed film was present (Fig. 4d). Note that it is difficult to derive the size of the particles from these experiments. The maximum lateral resolution of BAM is 0.2 µm; therefore, the occurrence of larger and smaller particles at the same time leads to a superposition of particles which can be regularly depicted and those which are smaller than the resolution of the microscope. The latter are observed as Newtonian rings. Therefore, the fine structure in Fig. 4d can be misleading.

If the pure solid-condensed stearic acid monolayer was expanded and compressed several times, the closed surface ruptured and solid condensed domains of the lipid surrounded by gas-analogue regions evolved. If the Ca $(HCO_3)_2$ solution was injected below such a film, crystallization took place only underneath the solid condensed domains (Fig. 5). It is interesting to note that the growth of these crystal films was not simply initiated beneath the domains and then continued in all directions. In contrast, it

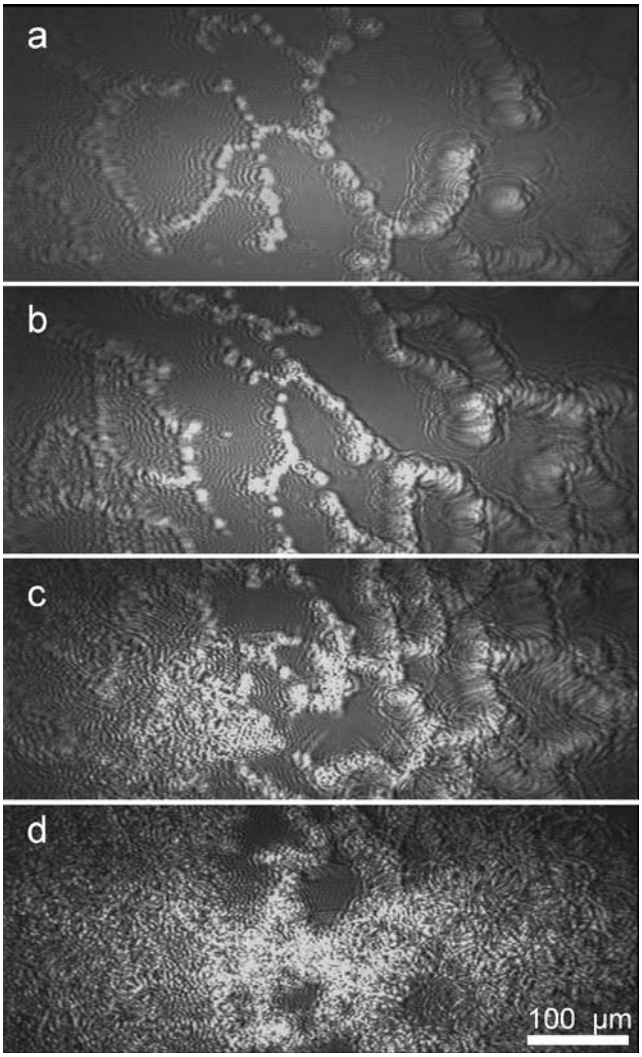

Fig. 4 Growth of a thin film of $CaCO_3$ below a stearic acid monolayer (Π_o=35 mN m^{-1}, T=22 °C, pH=7); **a** 0 min, **b** 3 min, **c** 6 min, **d** 12 min

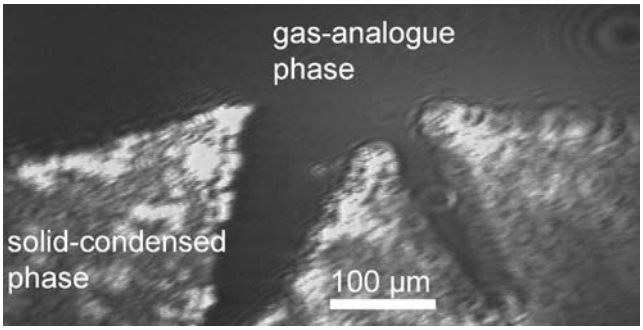

Fig. 6 Fracturing of the $CaCO_3$ thin film shown in Fig. 5 after expansion (Π_o≈5 mN m^{-1}, T=20 °C, [$Ca(HCO_3)_2$]=2 mM, pH=7)

appeared to be controlled by the shape of the domains, e.g. the growth of $CaCO_3$ films was never detected outside the boundaries of the solid-condensed domains.

When the expanding and compressing steps were carried out after the formation of the $CaCO_3$ crystals, we observed the fracture of these films (Fig. 6). The shape of the broken structures was completely different from the observations made for pure surfactant monolayers. Monolayer domains of stearic acid have round shapes and are prone to re-orientation. Expansion processes after crystal formation induced a break-up into sharp structures (Fig. 5). Thus, it can be assumed that the observed films were brittle. So it can be concluded that the stearic acid monolayers and the $CaCO_3$ sublayers were firmly adhering.

To simplify the observed system, we replaced the Ca$(HCO_3)_2$ solutions with an aqueous solution of Silica Ludox® particles. It is well known that $CaCO_3$ particles have a negative zeta potential [55]. Typical diameters of 15 nm for $CaCO_3$ primary particles were reported in recent publications [56]. In this respect, Silica Ludox® particles provide a good model system for primary $CaCO_3$ particles (behaving like nuclei for crystallization). In a series of

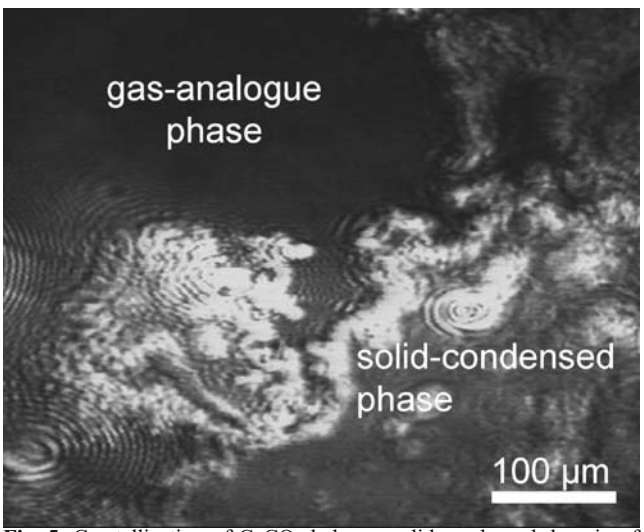

Fig. 5 Crystallization of $CaCO_3$ below a solid-condensed domain of stearic acid (Π_o≈5 mN m^{-1}, T=20 °C, [$Ca(HCO_3)_2$]=2 mM, pH=7)

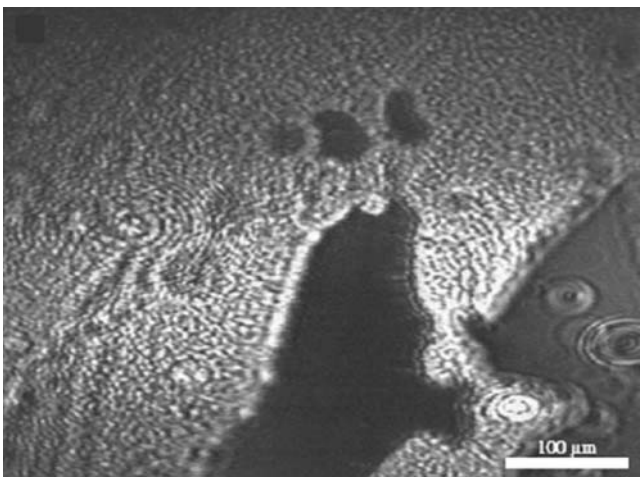

Fig. 7 A solid condensed domain of stearic acid with adhering Silica Ludox® beads (Π_o≈5 mN m^{-1}, T=20 °C, [Silica Ludox®]≈2 g l^{-1}, pH=7)

Table 1 Summary of all crystallization experiments performed below different monolayers and observed with BAM

Formation of $CaCO_3$ thin films	
Observed	Stearic acid
	TCDA
Not observed	Stearylalcohol
	Stearylamine
	Stearylsulfate
	DMPC

experiments, we repeated the surface-induced crystallization processes. It turned out that the Silica Ludox® particles behaved in the same way as the $CaCO_3$ primary crystals. The particles formed aggregates and thin films below solid condensed films of stearic acid. In this case, the formation of these thin films was also controlled by the boundaries of the solid-condensed domains (Fig. 7). The fact that the silica particles showed the same aggregation behaviour like the calcium carbonate crystals suggests that this process is in fact an aggregation of previously formed nanoparticles and not an epitactic crystallization of calcium carbonate below the Langmuir film. The evident attraction to defects and solid condensed films remains to be explained at this stage.

In addition to stearic acid, other surfactants like stearylalcohol, stearylamine, DMPC and TCDA were studied. The results of these experiments are summarized in Table 1.

It is evident that the formation of thin films was favoured in the presence of carboxy head groups. For thin films of stearylsulfate, which are also negatively charged, we observed only isolated crystals. This is possibly due to the high acidity of the sulfate groups as well as the weaker interactions with calcium ions. From biological mineralization processes, it is well known that carboxyl groups play an important role in guiding biomineralization processes [1].

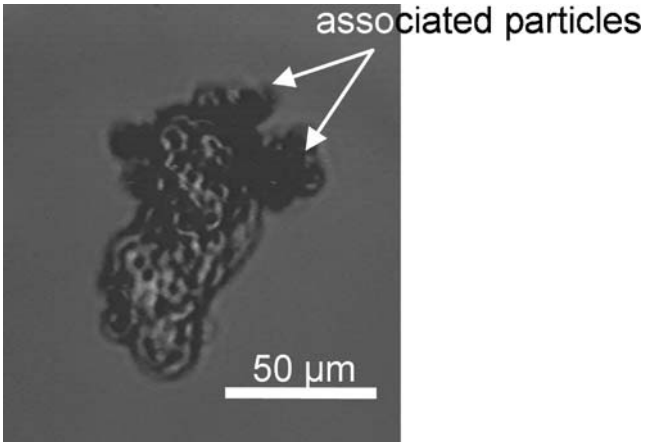

Fig. 9 Irregular object below a stearic acid monolayer, observed by light microscopy ($\Pi_o \approx 25$ mN m^{-1}, T=20 °C, [$Ca(HCO_3)_2$]=4 mM, pH=7)

Light microscopy

By light microscopy, we mainly observed the formation of single objects which can possibly be associated with calcite and vaterite crystals (see also the results of SEM below). In addition to these objects, we also detected larger structures of associated particles which had grown below the monolayer of stearic acid (Fig. 8). These objects had a random shape, and smaller, single particles aggregated onto these (see the arrows in Fig. 9). By their size and shape, these larger structures can most likely be associated with the $CaCO_3$ thin films, although no direct evidence can be derived from mere optical comparison.

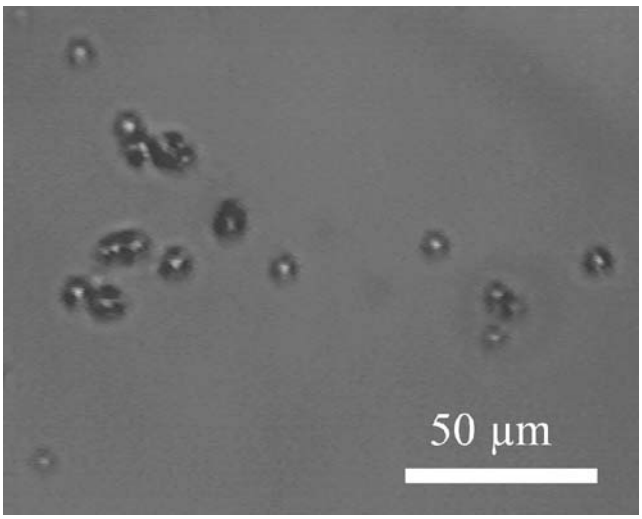

Fig. 8 Isolated particles below a stearylalcohol monolayer, observed by light microscopy ($\Pi_o \approx 25$ mN m^{-1}, T=20 °C, [$Ca(HCO_3)_2$]=4 mM, pH=7)

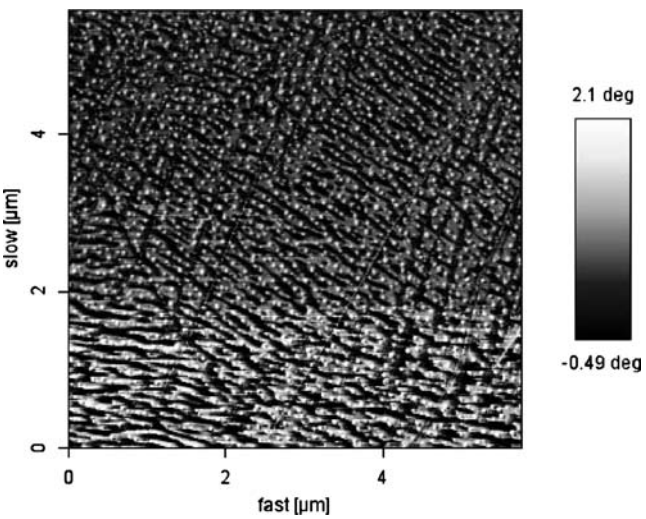

Fig. 10 AFM phase profile image of $CaCO_3$ particles formed below a monolayer of stearic acid (Π_o=30 mN m^{-1}, T=20 °C, [$Ca(HCO_3)_2$]=4 mM, pH=7)

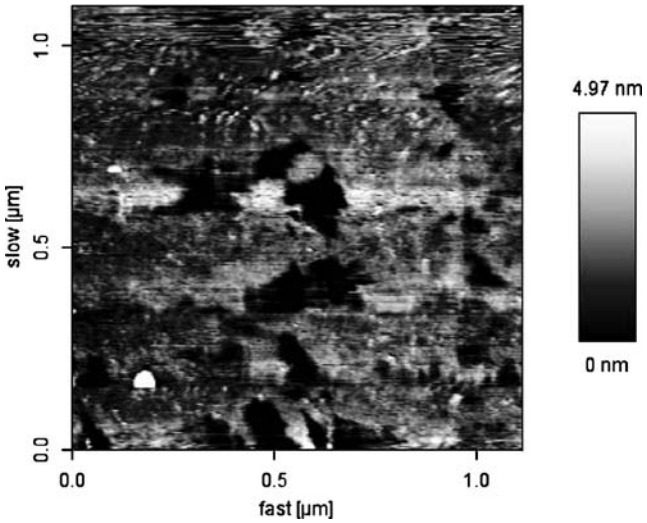

Fig. 11 AFM height profile of a $CaCO_3$ film formed below a monolayer of stearic acid (Π_o=30 mN m^{-1}, T=20 °C, [$Ca(HCO_3)_2$]=4 mM, pH=7)

Atomic force microscopy

By AFM, the growth of single particles and the formation of thin films could both be observed. The particles appeared as bright spheres with a height of about 5 nm (Fig. 10, height derived from corresponding height-profile) above the lipid monolayer [57]. On the phase picture, the particles showed a strong contrast to the surfactant monolayer, which suggests that the particles indeed consisted of calcium carbonate and not of lipid multilayers. The surfactant monolayer showed many defects which may be induced by the Langmuir–Blodgett technique. These phenomena may also be due to the weak attachment of the hydrophobic tails of the lipids to the graphite substrate.

The $CaCO_3$ thin films which were observed on BAM images may be related to the structures shown in Fig. 11 by AFM. In this paper, a very rough surface with many holes was observed. The maximum depth of the uneven surface was of the order of 12 nm (obtained from cross-section). This may correspond to the minimum thickness of the $CaCO_3$ films. Again there is no direct evidence for the analogy, but because the structure shown in Fig. 11 matches very well with the surface structure of the object shown in Fig. 12b, this comparison is further substantiated.

Scanning electron microscopy

A summary of the different results is shown in Table 2.

By means of scanning electron microscopy (SEM), a more detailed inspection of the observed structures was possible. The selected images provide a close look onto the crystal shapes and surfaces. However, it is more difficult to get information by SEM about the height or the thickness of the films. The structures observed in this paper can be compared to those described above. Generally, the dark, plane regions represent the lipid monolayer with the head groups facing towards the observer. As reported earlier [7–9, 54], calcite and vaterite crystals were observed, depending on the experimental conditions (see Table 2). In this paper, attention is drawn to the more irregular yet reproducible structures. All of the presented objects consisted of calcium carbonate as verified by quantitative EDX analysis and were observed rather seldom but reproducibly. At 20 °C, we observed large, layered structures in the vicinity of single crystals (Fig. 12a). A closer inspection of the surface of these objects revealed that these structures consisted of calcium carbonate aggregates, composed of small particles with a diameter of about 30–60 nm (Fig. 12b). Because of the special size and shape of these structures, they can be associated with the $CaCO_3$ object shown in Fig. 9. Like in Fig. 9, a single crystal (here, calcite) is surrounded by smaller objects. By light microscopy, it could be observed that single crystals were often

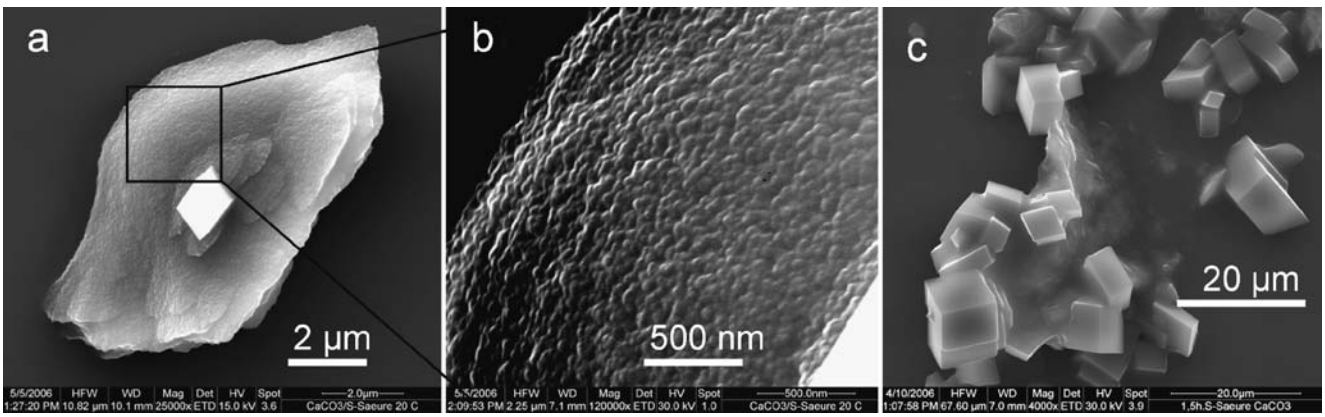

Fig. 12 **a**, **b** SEM image of a calcium carbonate film formed below a monolayer of stearic acid. Note the multilayered structure and the calcite single crystal on top of the film. The structure consists of small particles with typical diameter of 50 nm. T=20 °C, [$Ca(HCO_3)_2$]=6 mM, t_{growth}=1.5 h, Π_o=30 mN m^{-1}, pH=7). **c** A cluster of calcite crystals formed in a calcium carbonate thin film (T=20 °C, [$Ca(HCO_3)_2$]=6 mM, t_{growth}=1.5 h, Π_o=30 mN m^{-1}, pH=7)

Table 2 Summary of all SEM studies carried out on crystallization experiments

Temperature (°C)	$[Ca(HCO_3)_2]$/mM	pH	Particle density	t_{growth}	Calcite	Vaterite	Leaf-like objects	Aggregates
5	6	7	Low	1.5 h	Yes	Yes	Regularly	No
10	6	7	Low	1.5 h	Yes	Yes	Seldom	No
15	6	7	Medium	1.5 h	Yes	Yes	No	Yes
20	6	7	High	1.5 h	Yes	Yes	No	Yes
25	6	7	High	1.5 h	Yes	Often	No	Often
35	6	7	High	1.5 h	Yes	More often	No	Often
40	6	7	Low	1.5 h	Yes	Seldom	No	Yes
20	0.5	7	No particles	1.5 h	No	No	No	No
20	1	7	Low	1.5 h	Yes	Yes	Yes	No
20	2	7	Low	1.5 h	Yes	Yes	Yes	No
20	4	7	Medium	1.5 h	Yes	Yes	Seldom	Seldom
20	5	7	Medium	1.5 h	Yes	Yes	No	Seldom
20	7	7	High	1.5 h	Yes	Yes	No	Often
20	8	7	High	1.5 h	Yes	Yes	Seldom	Very often
20	6	3.7	No particles	1.5 h	No	No	No	No
20	6	5,5	Very low	1.5 h	Yes	No	No	No
20	6	8	Very high	1.5 h	Yes	Yes	No	Yes
20	6	7	Low		10 min	Seldom	Yes	No
No								
20	6	7	Medium		30 min	Yes	Yes	No
Yes								
20	6	7	Medium	2 h	Yes	Seldom	No	Often
20	6	7	Low	2.5 h	Yes	No	No	Seldom
20	6	7	Very low	1 day	Yes	No	No	Yes

The monolayer was composed of 150 μL of 1 mM stearic acid, spread from $CHCl_3$-solution and compressed to 30 mN m^{-1}. The polymorphic phases were identified by their external morphology. Aragonite was generally excluded due to preceding X-ray powder diffraction experiments (see text).

found in contact with these larger objects. The reason why only few of these objects can be observed could be that they are metastable. Over time, they may develop into branched vaterite crystals (Fig. 14a), or they are forming clusters of grown-out calcite or vaterite crystals (Fig. 12c). This is concluded by comparison of the structures from BAM and SEM, as it is impossible to observe phase transitions under these conditions (in the given time frame) because of the lack of water.

At a lower temperature of 5 °C, a large number of leaf-like structures was observed. Again, these objects consisted of smaller particles which had typical diameters between 50 and 100 nm. Similar structures could be observed at very low subphase concentrations (see Table 2 and Fig. 14c). The structures on the lower side of the lower "leaf" shown in Fig. 13a resemble small vaterite-flower-crystals in an early growth state (compare to Fig. 14a). In addition, the whole leaf-like structure resembles the object shown in

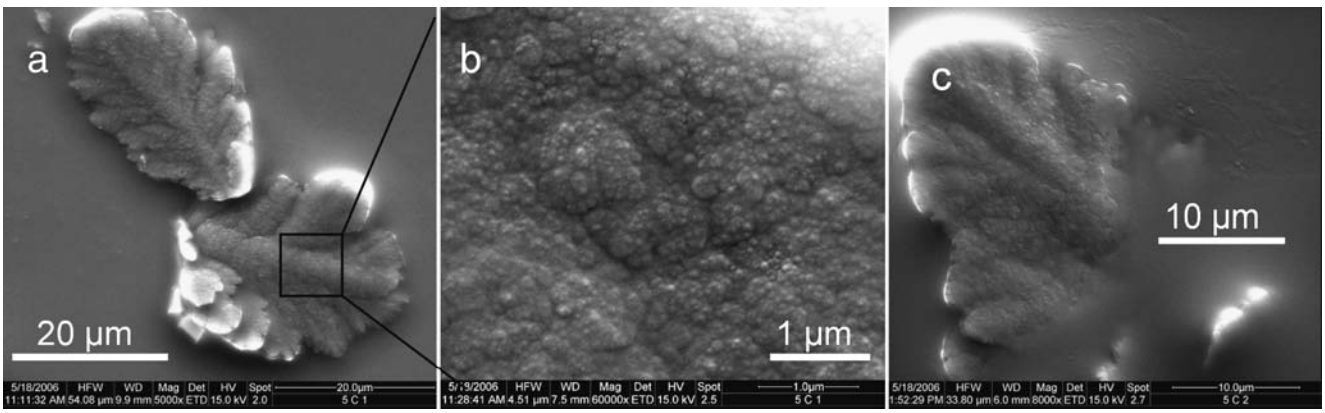

Fig. 13 Typical SEM images of leaf-like calcium carbonate films formed below a monolayer of stearic acid at T=5 °C, $[Ca(HCO_3)_2]$=6 mM, t_{growth}=1.5 h, Π_o=30 mN m^{-1}, pH=7. The films consist of small particles with typical diameters between 50 and 100 nm

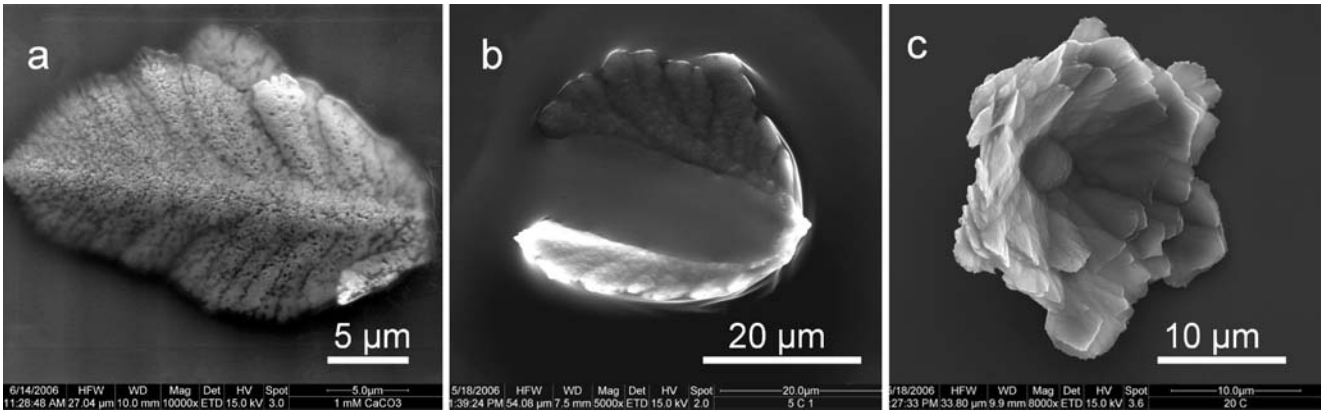

Fig. 14 Vaterite crystals. **a** fully grown, formed at T=20 °C, [Ca$(HCO_3)_2$]=6 mM, t_{growth}=1.5 h, Π_o=30 mN m^{-1}, pH=7; **b** early growth state at 5 °C, [Ca$(HCO_3)_2$]=6 mM, t_{growth}=1.5 h, Π_o=30 mN m^{-1}, pH=7; **c** Leaf-like calcium carbonate structure obtained at [Ca$(HCO_3)_2$]=1 mM, T=20 °C, t_{growth}=1.5 h, Π_o=30 mN m^{-1}, pH=7

Fig. 14b, which is probably a vaterite crystal in an early growth state (many similar structures were found which more or less resembled vaterite crystals). So it may be assumed that these objects are metastable intermediates or precursor aggregates which are trapped in this state because of the removal of water. Again, this is concluded only by analogy. The size of the particles from which these structures are formed is about 50–100 nm. From these observations, it could also be concluded that the primary calcium carbonate particles are more stable at lower temperatures or very low subphase concentrations.

Under these assumptions, these structures can be explained by mechanisms of colloidal growth processes. In other words, an organization process on the mesoscale through the assembly of calcium carbonate nanoparticles is assumed [15]. The polymorphic phase of these primary particles could not be determined in these experiments due to the small amount of substance available.

Conclusions

Regarding the aggregation processes of $CaCO_3$ primary particles as well as of Silica Ludox® particles, there are still some basic questions unresolved. Because both structures have a net negative surface charge, adsorption and aggregation processes to the negatively charged stearic acid film appear to be energetically unfavourable. In this paper, the accumulation of the particles in proximity to the monolayer can only be induced by the compensation of the negative charges on the particle surfaces. This can be achieved by positively charged counterions that adsorb on the surface of

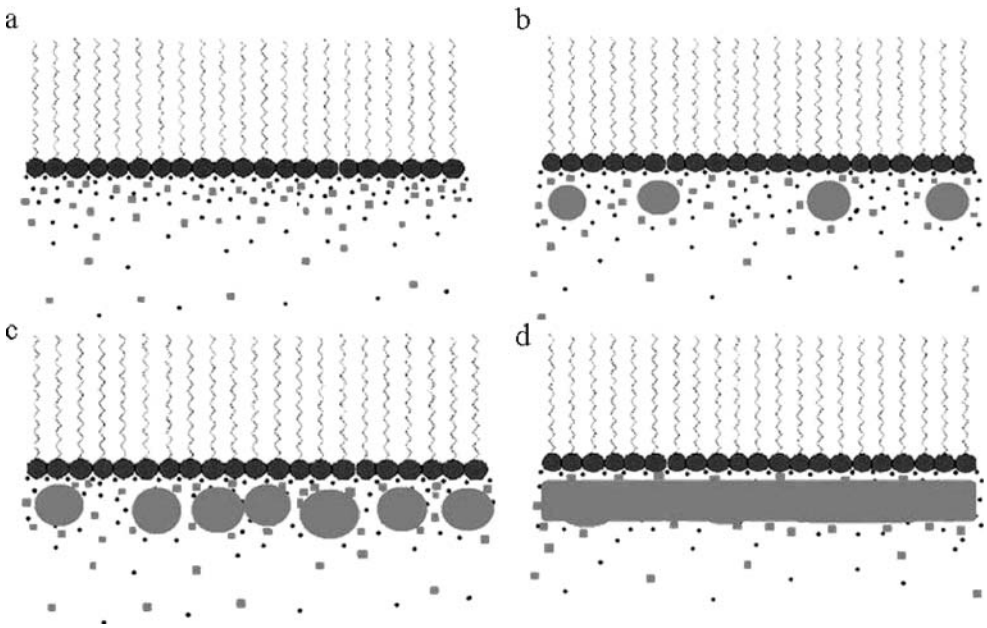

Fig. 15 Schematic picture of the formation of a $CaCO_3$ thin film under a monolayer of stearic acid. *Small gray dots* Calcium and carbonate ions, *light gray* calcium carbonate precursor particles and film

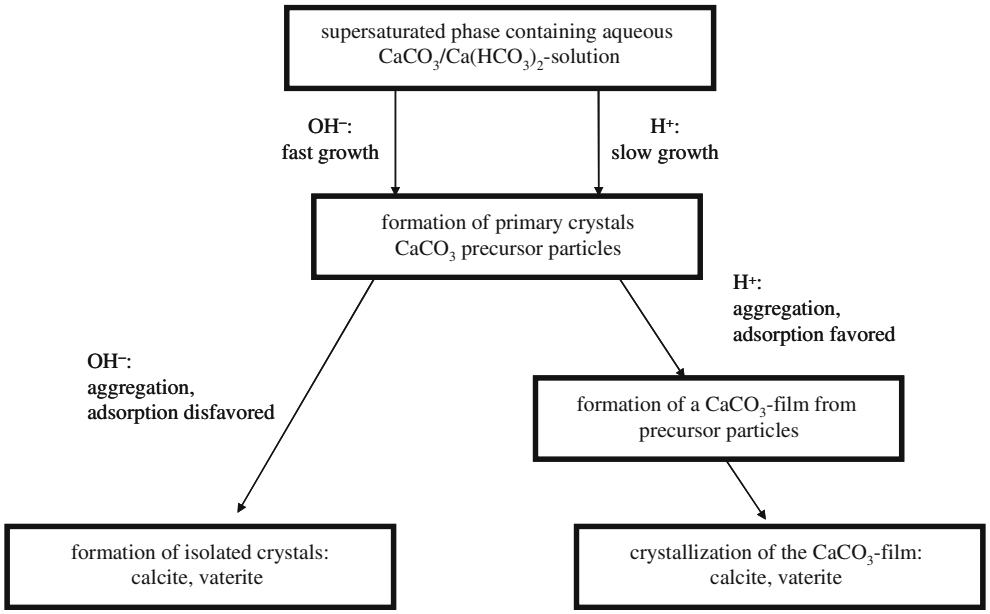

Scheme 1 Proposed model for the formation of $CaCO_3$ thin films

the nanoparticles. In monolayers of fatty acids, protons can be supplied by the carboxylic head groups, and cations from the subphase can be accumulated. Thus the surface charge of the particles can be reduced or compensated so that the particles become able to absorb at the monolayer. Concerning the formation of $CaCO_3$ crystals, another electrostatic effect has to be taken into account. This becomes clear by considering the following reaction:

$$Ca^{2+}(aq) + 2HCO_3^-(aq) \leftrightarrow Ca^{2+}(aq) + 2CO_3^{2-}(aq) + 2H^+(aq) \quad (2)$$

If the proton concentration is increased, the equilibrium shown in this equation shifts to the left. That means that the formation of $CaCO_3$ crystals is disfavoured. It may be possible that this also means that the stability of the primary particles, which form before grown-out $CaCO_3$ crystals occur [14, 16], increases. Note that only the proton concentration in proximity to the head groups of the lipids is concerned. If the bulk pH is altered (see Table 2), the crystallization is no longer controlled by the interface. The observed formation of the $CaCO_3$ thin films can be described as presented in Fig. 15: Below the stearic acid monolayer, a supersaturation of calcium and hydrogencarbonate ions occurs (Fig. 15a). From this supersaturated phase in proximity to the Langmuir film, calcium carbonate particles form (Fig. 15b). From this point, the mechanism may proceed in two directions. First, out of the particles, the formation of crystallites occurs. This was observed for monolayers of stearylalcohol. Second, if the primary particles remain stable for a longer period of time, the particles can aggregate (Fig. 15c) and form a thin film. This precursor film finally converts into more stable $CaCO_3$ modifications, like leaf-like structures, vaterite-flower-crystals or clusters of well-developed calcite crystals and vaterite crystal agglomerations (Fig. 15d). A simple model describing all these features is summarized in Scheme 1.

Acknowledgements Special thanks are due to Ursula Giebel for the performance of the SEM-measurements.

References

1. Baeuerlein E (2000) Biomineralization. Wiley-VCH, Weinheim
2. Baeuerlein E (2003) Angew Chem Int Ed 42:614–641
3. Baeuerlein E (2004) Biomineralization. Progress in biology, molecular biology and application. Wiley-VCH, Weinheim, New York
4. Lowenstam HA, Weiner S (1989) On biomineralization. Oxford University Press, New York
5. Mann S (2001) Biomineralization; principles and concepts in bioinorganic materials chemistry. Oxford University Press, Oxford
6. Meldrum FC (2003) Int Mater Rev 48:187–224
7. Heywood BR, Mann S (1994) Chem Mater 6:311–318
8. Mann S, Heywood BR, Rajam S, Walker JBA (1991) J Phys D-Appl Phys 24:154–164
9. Mann S, Archibald DD, Didymus JM, Douglas T, Heywood BR, Meldrum FC, Reeves NJ (1993) Science 261:1286–1292
10. DiMasi E, Olszta MJ, Patel VM, Gower LB (2003) CrystEngComm 5:346–350
11. Duffy DM, Harding JH (2004) Langmuir 20:7637–7642
12. Liu XY, Lim SW (2003) J Am Chem Soc 125:888–895
13. Lochhead MJ, Letellier SR, Vogel V (1997) J Phys Chem B 101:10821–10827
14. Ogino T, Suzuki T, Sawada K (1987) Geochim Cosmochim Acta 51:2757–2767
15. Colfen H, Mann S (2003) Angew Chem Int Ed 42:2350–2365
16. Olszta MJ, Odom DJ, Douglas EP, Gower LB (2003) Connect Tissue Res 44:326–334
17. Raz S, Weiner S, Addadi L (2000) Adv Mater 12:38–42
18. Addadi L, Raz S, Weiner S (2003) Adv Mater 15:959–970
19. Aizenberg J, Lambert G, Weiner S, Addadi L (2002) J Am Chem Soc 124:32–39

20. Boskey AL (2003) Connect Tissue Res 44:5–9
21. Colfen H (2003) Curr Opin Colloid Interface Sci 8:23–31
22. Hasse B, Ehrenberg H, Marxen JC, Becker W, Epple M (2000) Chem Eur J 6:3679–3685
23. Marxen JC, Becker W, Finke D, Hasse B, Epple M (2003) J Molluscan Stud 69:113–121
24. Volkmer D, Fricke M, Agena C, Mattay J (2004) J Mater Chem 14:2249–2259
25. Colfen H, Antonietti M (2005) Angew Chem Int Ed 44:5576–5591
26. Horn D, Rieger J (2001) Angew Chem Int Ed 40:4331–4361
27. Loste E, Meldrum FC (2001) Chem Commun 10:901–902
28. Günter C, Becker A, Wolf G, Epple M (2005) Z Anorg Allg Chem 631:2830–2835
29. Volkmer D, Harms M, Gower L, Ziegler A (2005) Angew Chem Int Ed 117:645–650
30. Aizenberg J, Lambert G, Addadi L, Weiner S (1996) Adv Mater 8:222–226
31. Albeck S, Weiner S, Addadi L (1996) Chem Eur J 2:278–284
32. Albeck S, Addadi L, Weiner S (1996) Connect Tissue Res 35:365–370
33. Becker A, Becker W, Marxen JC, Epple M (2003) Z Anorg Allg Chem 629:2305–2311
34. Belcher AM, Wu XH, Christensen RJ, Hansma PK, Stucky GD, Morse DE (1996) Nature 381:56–58
35. Blank S, Arnoldi M, Khoshnavaz S, Treccani L, Kuntz M, Mann KH, Grathwohl G, Fritz M (2003) J Microsc 212:280–291
36. Coblentz FE, Shafer TH, Roer RD (1998) Comp Biochem Physiol Part B Biochem Mol Biol 121:349–360
37. Falini G, Albeck S, Weiner S, Addadi L (1996) Science 271:67–69
38. Feng QL, Pu G, Pei Y, Cui FZ, Li HD, Kim TN (2000) J Cryst Growth 216:459–465
39. Gotliv BA, Weiner S, Addadi L (2003) ChemBioChem 4:529
40. Raz S, Hamilton PC, Wilt FH, Weiner S, Addadi L (2003) Adv Funct Mater 13:480–486
41. Wada N, Okazaki M, Tachikawa S (1993) J Cryst Growth 132: 115–121
42. Wheeler AP, George JW, Evans CA (1981) Science 212: 1397–1398
43. Zaremba CM, Belcher AM, Fritz M, Li Y, Mann S, Hansma PK, Morse DE, Speck JS, Stucky GD (1996) Chem Mater 8:679–690
44. Hoch AR, Reddy MM, Aiken GR (1999) Geochim Cosmochim Acta 64:61–72
45. Manoli F, Dalas E (1999) J Cryst Growth 217:416–421
46. Teng HH, Dove PM, Orme CA, de Yoreo JJ (1998) Science 282:724–727
47. Jin DH, Zhang Y, Nagunuma T, Ogawa T, Hatekakeyama E, Muramoto K (2000) J Agric Food Chem 48:5454
48. Volkmer D, Fricke M, Huber T, Sewald N (2004) Chem Commun 4579–4582
49. Colfen H, Qi L (2001) Adv Mater 14:300–303
50. Hacke S (2001) Brewsterwinkel-Mikroskopie zur Untersuchung der Kristallisation von Calciumcarbonaten an Modell-Monofilmen an der Grenzfläche Wasser/Luft. Ph.D. thesis, University of Göttingen, Germany
51. Hacke S, Möbius D (2004) Colloid Polym Sci 282:1242–1246
52. Backov R, Lee CM, Khan SR, Mingotaud C, Fanucci GE, Talham DR (2000) Langmuir 16:6013–6019
53. Benitez IO, Talham DR (2004) Langmuir 20:8287–8293
54. Buijnsters PJJA, Donners JJJM, Hill SJ, Heywood BR, Nolte RJM, Zwanenburg B, Sommerdijk NAJM (2001) Langmuir 17: 3623–3628
55. Moulin P, Roques H (2003) J Colloid Interface Sci 261:115–126
56. Donnet M, Bowen P, Jongen N, Lemaitre J, Hofmann H (2005) Langmuir 21:100–108
57. Müller H, Zentel R, Janshoff A, Janke M (2006) Langmuir 22: 11034–11040